Journal Pre-proofs

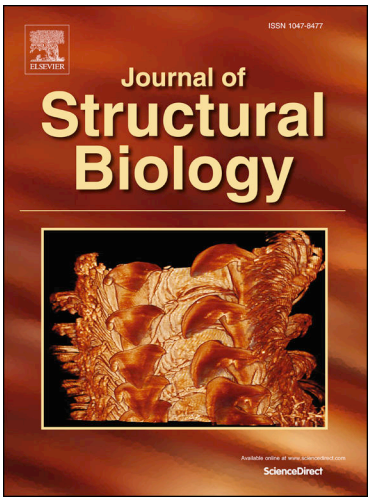

Research Article

Structural and biochemical insights into His-tag-induced higher-order oligomerization of membrane proteins by cryo-EM and size exclusion chromatography

Nooraldeen Ayoub, Patrick Roth, Zöhre Ucurum, Dimitrios Fotiadis, Stephan Hirschi

PII: S1047-8477(22)00094-6
DOI: https://doi.org/10.1016/j.jsb.2022.107924
Reference: YJSBI 107924

To appear in: *Journal of Structural Biology*

Received Date: 7 August 2022
Revised Date: 18 November 2022
Accepted Date: 26 November 2022

Please cite this article as: Ayoub, N., Roth, P., Ucurum, Z., Fotiadis, D., Hirschi, S., Structural and biochemical insights into His-tag-induced higher-order oligomerization of membrane proteins by cryo-EM and size exclusion chromatography, *Journal of Structural Biology* (2022), doi: https://doi.org/10.1016/j.jsb.2022.107924

Structural and biochemical insights into His-tag-induced higher-order oligomerization of membrane proteins by cryo-EM and size exclusion chromatography

Nooraldeen Ayoub[1,‡], Patrick Roth[1,‡], Zöhre Ucurum[1], Dimitrios Fotiadis[1,*], Stephan Hirschi[1,*,+]

[1] Institute of Biochemistry and Molecular Medicine, University of Bern, Bühlstrasse 28, 3012 Bern, Switzerland

[+] Present address: Department of Biochemistry, University of Oxford, South Parks Road, Oxford OX1 3QU, United Kingdom

[‡] Contributed equally to this work and share first authorship

[*] To whom correspondence may be addressed: Dimitrios Fotiadis (dimitrios.fotiadis@ibmm.unibe.ch) or Stephan Hirschi (stephan.hirschi@bioch.ox.ac.uk)

Abstract

Structural and functional characterization of proteins as well as the design of targeted drugs heavily rely on recombinant protein expression and purification. The polyhistidine-tag (His-tag) is among the most prominent examples of affinity tags used for the isolation of recombinant proteins from their expression hosts. Short peptide tags are commonly considered not to interfere with the structure of the tagged protein and tag removal is frequently neglected. This study demonstrates the formation of higher-order oligomers based on the example of two His-tagged membrane proteins, the dimeric arginine-agmatine antiporter AdiC and the pentameric light-driven proton pump proteorhodopsin. Size exclusion chromatography revealed the formation of tetrameric AdiC and decameric as well as pentadecameric proteorhodopsin through specific interactions between their His-tags. In addition, single particle cryo-electron microscopy (cryo-EM) allowed structural insights into the three-dimensional arrangement of the higher-order oligomers and the underlying His-tag-mediated interactions. These results reinforce the importance of considering the length and removal of affinity purification tags and illustrate how neglect can lead to potential interference with downstream biophysical or biochemical characterization of the target protein.

Keywords: cryo-EM, His-tag, membrane protein, oligomerization, protein aggregation, size exclusion chromatography

Abbreviations: cryo-EM, cryo-electron microscopy; Cymal-5, 5-cyclohexyl-1-pentyl-β-D-maltoside; DM, n-decyl-β-D-maltoside; GPR, green-light absorbing proteorhodopsin; His-tag, polyhistidine-tag; IMAC, immobilized metal ion affinity chromatography; MW, molecular weight; SDS-PAGE, sodium dodecyl sulphate-polyacrylamide gel electrophoresis; SEC, size exclusion chromatography.

Introduction

Immobilized metal ion affinity chromatography (IMAC) of His-tagged proteins has become a principal tool to purify recombinant proteins for structural and functional studies (Hochuli et al., 1988). Developments in genetic engineering have allowed the specific isolation of His-tagged target proteins from a wide range of expression systems. The most frequently employed His-tag variant is the hexahistidine-tag (His_6-tag), but shorter and longer histidine sequences have found successful application as well. The number of histidines has been shown to correlate with a protein's affinity to immobilized metal ions (Bornhorst and Falke, 2000; Hemdan et al., 1989; Mohanty and Wiener, 2004). Consequently, longer repeats, such as His_8- or His_{10}-tags, allow more stringent washing conditions for the removal of non-specifically bound contaminants and can thus potentially yield higher protein purity. This is particularly beneficial when working with specific expression hosts that contain endogenous metal chelating proteins or histidine-rich proteins, which efficiently bind to the IMAC column (Bolanos-Garcia and Davies, 2006; Kaur and Reinhardt, 2012; Schmitt et al., 1993; Wülfing et al., 1994). In addition, longer His-tags can also significantly improve the purification of proteins with low expression levels, both in terms of purity and yield (Bergeron et al., 2011; Boggavarapu et al. 2013; Grisshammer and Tucker, 1997). On the other hand, the His_{10}-tag has been shown to induce the formation of higher-order oligomers and protein aggregation (Mohanty and Wiener, 2004). Tag-induced aggregation will interfere with the downstream biophysical or biochemical characterization of the target protein, yielding ambiguous results that are prone to misinterpretation. This can lead to wrong assumptions about the apparent molecular weight (MW) and oligomeric assembly of the protein, and can impede structure determination if the tag is not removed. Thus, a common practice is the proteolytic removal of affinity purification

tags using specifically introduced protease cleavage sequences (Hirschi and Fotiadis, 2020; Waugh, 2011). The cleavage efficiency can be drastically reduced by oligomerization of the tagged protein, which may affect the accessibility of the protease (Hirschi et al., 2020; Kenig et al., 2006). It is thus essential to evaluate the length of the His-tag and desired removal method to ensure optimal conditions for protein purification and characterization.

Here, we showcase examples of two membrane proteins purified using a His_{10}-tag, which induced the formation of non-physiological higher-order oligomers. This issue was investigated using the dimeric arginine-agmatine antiporter AdiC from *Escherichia coli* and the pentameric green-light absorbing proteorhodopsin (GPR), a light-driven proton pump from γ-proteobacteria. Different constructs were used to investigate the effect of the presence and length of a His-tag on the homogeneity of the protein samples. Size exclusion chromatography (SEC) and single particle cryo-electron microscopy (cryo-EM) were used to gain insights into the structural and biochemical basis of higher-order oligomer formation, which revealed that interactions between physiological oligomers are directly mediated by their His-tags.

Results and discussion

Higher-order oligomer formation depends on the presence and length of His-tags

IMAC purification of C-terminally His_{10}-tagged AdiC solubilized in n-decyl-β-D-maltoside (DM) combined with on-column human rhinovirus (HRV) 3C protease cleavage, to remove the tag, or elution with L-histidine yielded highly pure protein

samples (Figure 1a and b). Both, uncleaved and cleaved AdiC ran as single bands on SDS-polyacrylamide gels at about 36 kDa and 34 kDa, respectively, confirming successful proteolytic removal of the His_{10}-tag. In both cases, the proteins migrated faster than expected from the MW of the AdiC monomers (calculated molecular weight $(MW)_{uncleaved}$ = 49.8 kDa; calculated $MW_{cleaved}$ = 48.0 kDa), a common behaviour for membrane proteins (Rath et al., 2009; Reig et al., 2007; Weitz et al., 2007).

To assess how the presence of a His-tag affects the oligomeric assembly of AdiC, constructs with and without C-terminal His_{10}-tag were analysed by SEC (Figure 1). Uncleaved AdiC eluted with L-histidine was found to be a heterogeneous mixture of two populations, with a main peak at an elution volume (V_e) of ~15.5 mL and a fronting shoulder at ~14.4 mL (Figure 1a). SEC can be used to approximate the apparent MW of a membrane protein (i.e., the protein-lipid-detergent complex) by comparison to the elution volumes of known MW marker proteins (Ilgü et al., 2014; Kunji et al., 2008). The apparent MWs of the two populations are about 168 kDa (V_e ~15.5 mL) and 297 kDa (V_e ~14.4 mL). The lower MW population corresponds to the known dimeric form of AdiC (Casagrande et al., 2008; Ilgü et al., 2014), whereas the higher MW population could represent a higher-order oligomer, e.g., a dimer of dimers. In contrast, proteolytic cleavage of the His_{10}-tag yielded highly homogenous AdiC dimers (Figure 1b), suggesting that formation of the higher MW population involves interactions mediated by the His_{10}-tag. This is further supported by the fact that formation of these potential tetramers could be prevented through competition with a high concentration (200 mM) of L-histidine during SEC (Figure 1c). Given this observed effect, complete removal of L-histidine (contained in the IMAC elution buffer, see materials and methods) from uncleaved AdiC samples prior to SEC might favour formation of tetrameric AdiC. Indeed, a more homogeneous higher MW population at an elution volume of ~13.9 mL

was observed when using desalted protein, providing a more reliable MW estimate for this AdiC oligomer species of about 384 kDa.

IMAC purification of 5-cyclohexyl-1-pentyl-β-D-maltoside (Cymal-5)-solubilized green-light absorbing proteorhodopsin with C-terminal His_{10}- (GPR-10H) or His_5-tag (GPR-5H) yielded highly pure protein samples, running as single bands on SDS-polyacrylamide gels at about 23 and 22 kDa, respectively (Figure 2a and b). As expected for membrane proteins, an anomalous migration behaviour similar to AdiC was observed for both GPR constructs (calculated $MW_{GPR\text{-}10H}$ monomer = 28.8 kDa and calculated $MW_{GPR\text{-}5H}$ monomer = 26.9 kDa). To complement the observations from AdiC, the effect of different His-tag lengths on the oligomeric assembly of GPR was assessed by SEC (Figure 2). Both GPR-10H and GPR-5H were found to be comprised of a heterogeneous mixture of two populations. They share the same lower MW population with V_e of ~16.7 mL (Figure 2), corresponding to a MW of about 89 kDa. However, the main peak in GPR-10H (V_e ~13.5 mL; Figure 2a) represents a significantly larger species than in GPR-5H (V_e ~15.2 mL; Figure 2b). Based on previous experiments, the lowest MW (V_e ~16.7 mL) population is attributed to monomeric GPR and the oligomeric form of GPR-5H (V_e ~15.2 mL) corresponds to a pentamer with a MW of about 196 kDa (Hirschi et al., 2020). Instead of a pentamer, a species with MW of about 473 kDa is found in the GPR-10H sample, which likely represents a higher-order oligomer, such as a dimer of pentamers. Additionally, this peak exhibits notable fronting compared to the pentamer peak, indicating the presence of even larger GPR assemblies. These results correlate with the observations made for AdiC, with both His_{10}-tagged proteins forming higher-order oligomers. In the case of AdiC, this could be prevented by proteolytic cleavage of the affinity tag. However, enzymatic tag removal for pentameric GPR is highly inefficient and a construct with a

shorter His_5-tag (GPR-5H) was designed instead. GPR-5H yielded a sharp pentamer peak, without traces of higher MW populations. Interestingly, preventing the His-tag interaction in GPR-10H using a high concentration of L-histidine during SEC was unsuccessful and did not affect the formation of all higher-order oligomers but only prevented the fronting, resulting in a more symmetrical oligomer peak (Figure 2c). This suggests that the GPR higher-order oligomers are held together by stronger interactions, mediated by a maximum of five His-tags in comparison to only two possible tags in AdiC. Collectively, SEC analysis of the AdiC and GPR constructs clearly demonstrate that longer His-tags bear the risk of inducing unwanted higher-order oligomers, which can be resolved to some degree by high L-histidine concentration or completely prevented by removal or shortening of the His-tag.

Structural insights into higher-order oligomer formation mediated by His_{10}-tags

His_{10}-tag constructs of AdiC and GPR have been found to form unexpectedly large assemblies using SEC. Based on their apparent MW, these higher-order oligomers potentially correspond to tetrameric AdiC and decameric GPR, which seem to be associated by specific interactions mediated by their His-tags (Figures 1 and 2). In order to gain more detailed insights into the oligomeric assembly and understand the underlying molecular interactions, the corresponding complexes were isolated by SEC (see materials and methods) and investigated by single particle cryo-EM analysis. Peak fractions of putative AdiC tetramers and GPR decamers were vitrified and datasets comprising 205 and 323 movies each were acquired on a cryo-electron microscope.

Electron micrographs of AdiC feature a homogenous particle distribution with two clearly discernible types (Figure 3a), consisting of either one or two closely associated elongated densities. For single particle analysis, about 50,000 particles were picked and subjected to several consecutive rounds of 2D classification to remove low-quality particles and contaminations. The final 2D class averages revealed smaller dimeric AdiC particles and larger particles formed by a stack of two dimers interacting at different angles (Figure 3b). This confirms the tetrameric assembly indicated by SEC (Figure 1). The C_2 symmetry-related homodimeric assembly of two AdiC protomers is clearly recognizable in all views. Top views of dimers resemble a pair of glasses, while side views exhibit a slightly curved, banana-like shape, which is preserved in the tetrameric assembly. Dimeric and tetrameric particle sets with 15,900 and 8,900 particles, respectively, were separated and individual *ab initio* 3D reconstructions were calculated. The resulting cryo-EM maps with resolutions of 10-15 Å were analysed by fitting a previously published high-resolution AdiC structure (Figures 3c and d) obtained by X-ray crystallography (Ilgü et al., 2021). A noticeable protrusion in the centre of the dimeric map is formed by the C-terminal His_{10}-tags. This coincides with the interaction interface in the tetrameric map, corroborating that tetrameric AdiC particles associate via their cytoplasmic sides, forming interactions between their His_{10}-tags. Higher resolution maps could not be obtained due to the limited particle number and, most importantly, due to the innate flexibility of the tetramer, as reflected by the different interaction angles between the dimers.

For single particle analysis of GPR about 40,300 particles were picked and processed analogously to the AdiC dataset. Three distinct particle populations representing physiological and higher-order oligomeric assemblies of GPR were identified on electron micrographs and 2D class averages (Figure 4a and b). The first two

populations consisted of native pentamers and decamers arising from two interacting pentamers (see two closely associated disk-shaped densities in Figure 4b). In addition, the dataset revealed an even larger oligomeric species, comprised of three adjacent, elongated densities consisting of three pentamers forming a pentadecamer. The relatively minor population of pentamers might originate from higher oligomers disrupted during sample preparation for cryo-EM, e.g., during protein concentration (materials and methods). Top views distinctly show the C_5-symmetry of pentameric particles as described previously (Hirschi et al., 2020). GPR decamers are comprised of two vertically stacked pentamers interacting at different angles, analogous to AdiC tetramers. Pentadecameric particles are formed by association of three GPR pentamers arranged into a trigonal shape around a common centre. The different oligomeric particle sets consisting of about 4,100 pentameric, 6,500 decameric and 3,200 pentadecameric particles were separated and used to calculate individual *ab initio* 3D reconstructions. This yielded cryo-EM maps with resolutions of 10-15 Å, which were fitted with a previously published structure of pentameric GPR (Figures 4c, d and e) obtained by single particle cryo-EM (Hirschi et al., 2021). Notably, the distance between the pentamers in decameric GPR (~40 Å) is larger than between the dimers in AdiC tetramers (~20 Å), which could be caused by greater heterogeneity in the corresponding 2D classes, i.e., different interaction angles between the pentamers. The pentadecameric particles are formed by a trigonal arrangement of three slightly inclined GPR pentamers, orienting their cytoplasmic sides towards a central connecting density. This confirms the presence of a species larger than decamers, which was already suggested by the observed fronting of the decameric GPR SEC peak (Figure 2a). The pentadecamer was found to form weaker interactions than the decamer and to dissociate upon addition of a high L-histidine concentration (200 mM), evident by the disappearance of the fronting (Figure 2c). Based on the presented three-

dimensional arrangement of GPR pentamers, this can likely be attributed to the skewed interaction angle, which provides a smaller interface than the flatter contact in the decamer and thus enables fewer tags to interact with each other.

Conclusion

Here, we have elucidated the effects of the presence and length of His-tags on the oligomeric assemblies of AdiC and GPR, two model membrane proteins with different stoichiometries. The formation of higher-order oligomers through specific interactions between His_{10}-tags was revealed by analysing complexes of different AdiC and GPR constructs using SEC. Following investigations by single particle cryo-EM allowed structural insights into the three-dimensional arrangement of these higher-order oligomers and the interactions mediating their assembly. His_{10}-tagged AdiC assembles into tetramers (dimers of dimers) and GPR into decamers and pentadecamers (dimers and trimers of pentamers), formed by direct interactions of the tags. However, none of these populations are observed when the His-tag is proteolytically removed or a shorter His_5-tag is used. This highlights the importance of selecting an appropriate length for the His-tag and considering its removal after affinity purification, and prior to biochemical and structural studies. Overall, these results corroborate that the formation of higher-order oligomers is directly correlated with the presence and length of His-tags. Since the formation of higher-order oligomers is induced through His-tag-specific interactions, this phenomenon is likely not limited to membrane proteins but could affect any recombinant His_{10}-tagged protein.

Materials and methods

Cloning and overexpression of AdiC and GPR

AdiC (GenBank: CP099588.1) and GPR (GenBank: AY601905.1) genes were cloned into the previously described pZUDF21 plasmid vector (Ilgü et al., 2014). The AdiC wild-type (WT) gene was engineered to encode for a C-terminal human rhinovirus (HRV) 3C protease cleavage site and a His_{10}-tag (AdiC WT-LEGGS-HRV3C-10H). The GPR WT gene was truncated by removing its 18 amino acid N-terminal signal sequence ($GPR_{\Delta 18}$) and was further engineered to yield a C-terminally His_{10}-tagged variant with a HRV 3C cleavage site similar to AdiC and a shorter His_5-tagged version ($GPR_{\Delta 18}$-LEGGS-HRV3C-10H and $GPR_{\Delta 18}$-LEG-5H).

E. coli BL21 (DE3) pLysS cells were transformed with the pZUDF21-AdiC construct and Rosetta 2 (DE3) cells with the pZUDF21-GPR-5H or pZUDF21-GPR-10H constructs. All transformed strains were grown in an orbital shaker at 37°C and 180 rpm (Multitron, Infors HT) in LB medium supplemented with 100 µg/mL ampicillin and 34 µg/mL chloramphenicol. Overexpression of AdiC was induced at an OD_{600} of 0.55 with 0.25 mM isopropyl-β-D-1-thiogalactopyranoside (IPTG) and cells were further grown for 4 h. For GPR cultures, the temperature was reduced to 18°C at an OD_{600} of 0.3-0.4 and overexpression was induced at an OD_{600} of 0.75 with 0.1 mM IPTG and 5 µM all-*trans* retinal (dissolved in ethanol). Cells were further grown overnight at 18°C.

Isolation of *E. coli* membranes

Cells overexpressing AdiC or GPR were harvested by centrifugation (Sorvall RC-5B centrifuge, DuPont Instruments) for 6 min at 10,000 × g and 4°C. The pellets were

resuspended in a total of 300-600 mL of membrane wash buffer (50 mM Tris-HCl adjusted to pH 8 at 4°C, 450 mM NaCl). The cells were washed by centrifugation for 8 min at 10,000 × g and 4°C and resuspending in <400 mL by shaking for 1 h at 200 rpm and 4°C, and then stored at -20°C until further use.

Frozen cells were thawed in a water bath (30°C) and incubated with a spatula tip of chicken egg white lysozyme powder (Apollo Scientific Ltd.) shaking for 10 min at 200 rpm and 4°C. Cells were lysed using a Microfluidizer M-110P (Microfluidics) by five passages at 1,500 bar. Cellular debris and unlysed cells were removed by centrifugation for 6 min at 10,000 × g and 4°C. Membranes containing the recombinant membrane proteins were harvested by ultracentrifugation (Optima L-90K ultracentrifuge, Beckman Coulter) for 1.5 h at 150,000 × g and 4°C. The pellet was washed twice by homogenization and centrifugation (1 h at 150,000 × g and 4°C) in membrane wash buffer. Finally, the pellet was resuspended and homogenized in purification buffer (for AdiC: 20 mM Tris-HCl pH 8 at 4°C, 300 mM NaCl, 10% (v/v) glycerol; for GPR: 20 mM HEPES-NaOH pH 7.5 at room temperature (RT), 300 mM NaCl, 10% (v/v) glycerol). Membranes were stored at -80°C until further use as 3 mL aliquots, representing the yield from 1 L of bacterial cell culture.

IMAC purification of AdiC and GPR

An AdiC membrane aliquot was thawed at RT and solubilized on a turnover shaker for 2 h at 4°C in 7 mL of purification buffer containing 2% (w/v) DM (Glycon Biochemicals). The solubilized sample was ultracentrifuged for 30 min at 100,000 × g and 4°C. The supernatant was added to 0.5 mL bed volume of equilibrated ProteinIso Ni-NTA Resin (TransGen) in a total of 7 mL purification buffer containing 5 mM L-histidine. AdiC was

bound to the resin for 2 h at 4°C on a turnover shaker and then transferred to a gravity-flow column (Promega). The column was washed three times with 7 mL of cold purification buffer containing 5 mM L-histidine and 0.2% (w/v) DM. Slight pressure was manually applied to the column with a syringe during washing. For proteolytic cleavage, the column was additionally washed with 2 mL of cold purification buffer containing 0.2% (w/v) DM to remove L-histidine. The buffer was then removed from the column by centrifugation (2,000 × g for 2 min at RT). To elute AdiC by on-column cleavage, the resin was incubated overnight on a turnover shaker at 4°C with 450 µL of purification buffer containing 0.2% (w/v) DM and 50 µL of His-tagged HRV 3C protease (~4 mg/mL) and then eluted by centrifugation (2,000 × g for 2 min at RT). Alternatively, AdiC was eluted by addition of 500 µL of elution buffer (20 mM Tris-HCl pH 8 at 4°C, 150 mM NaCl, 10% (v/v) glycerol, 0.2% (w/v) DM, 200 mM L-histidine) and incubation for 10 min at 4°C, followed by centrifugation (2,000 × g for 2 min at RT). To remove possible traces of co-eluted protease and uncleaved AdiC, the eluate was incubated for 15 min at 4°C on a turnover shaker with 100 µL of fresh resin pre-equilibrated with 0.2% (w/v) DM-containing purification buffer, transferred into a new column and eluted by centrifugation (2,000 × g for 2 min at RT). Protein concentration was measured spectrophotometrically at 280 nm with a NanoDrop OneC (Thermo Scientific) using the calculated mass extinction coefficients of uncleaved (1.73 $mL \cdot mg^{-1} \cdot cm^{-1}$) and cleaved AdiC (1.79 $mL \cdot mg^{-1} \cdot cm^{-1}$).

A GPR membrane aliquot was thawed at RT and solubilized on a turnover shaker overnight in the dark at 4°C in 7 mL of purification buffer containing 3% (w/v) Cymal-5 (Anatrace). The solubilized sample was ultracentrifuged for 40 min at 100,000 × g and 4°C. The supernatant was then added to 0.5 mL bed volume of equilibrated ProteinIso Ni-NTA Resin in a total of 7 mL purification buffer containing 60 mM imidazole. GPR

was bound to the resin at RT for 2 h on a turnover shaker protected from light and then transferred to a gravity-flow column. The column was washed three times with 7 mL of purification buffer containing 60 mM imidazole and 0.25% (w/v) Cymal-5. Finally, GPR was eluted with 1.5 mL of elution buffer (20 mM HEPES-NaOH pH 7.5 at RT, 150 mM NaCl, 10% (v/v) glycerol, 200 mM L-histidine, 0.25% (w/v) Cymal-5) added in 0.5 mL increments. Fractions of 200 µL were collected, dark red samples were pooled and the protein concentration was measured spectrophotometrically at 525 nm, the maximum absorbance wavelength of the retinal Schiff base. The experimental molar extinction coefficient of GPR is 45,000 $M^{-1} \cdot cm^{-1}$. The calculated MWs of retinal-bound GPR-10H and GPR-5H are 28,809 Da and 26,853 Da, respectively.

Size exclusion chromatography

For analytical SEC, one L-histidine-eluted AdiC sample was passed through a 2 mL Zeba Spin Desalting Column with 7 kDa MW cut-off (Thermo Scientific) to remove L-histidine while the other AdiC and GPR samples were analysed directly. Purified proteins were ultracentrifuged for 10 min at 200,000 × g and 4°C to remove possible insoluble protein aggregates prior to SEC. 220 µL of the protein samples at a concentration of 1.3-1.5 mg/mL were injected into an Äkta purifier (GE Healthcare) with a Superose 6 10/300 GL size exclusion column pre-equilibrated with SEC buffer (for AdiC: 20 mM Tris-HCl pH 8 at 4°C, 150 mM NaCl, 0.2% (w/v) DM; for GPR: 20 mM Bis-Tris propane-HCl pH 7.5 at 4°C, 150 mM NaCl, 0.25% (w/v) Cymal-5). The system was equipped with an UV-Vis detector, set to 280 nm and 525 nm for GPR or to 280 nm for AdiC, and connected to an automated fraction collector. To analyse the oligomeric assembly of AdiC and GPR in the presence of a high L-histidine

concentration, SEC buffers containing 200 mM L-histidine were used. Each panel in Figures 1 and 2 represents a purification of AdiC or GPR from one membrane aliquot.

For cryo-EM grid preparation (see below), purified uncleaved AdiC and GPR-10H were concentrated to ~125 µL using Amicon Ultra 0.5 mL 50 kDa centrifugal filter units (Millipore) and injected into an Äkta purifier equipped with a Superose 6 Increase 3.2/300 size exclusion column pre-equilibrated with SEC buffer. 100 µL SEC peak fractions of putative tetrameric AdiC and decameric GPR-10H were collected and concentrated to 2.6 and 2.3 mg/mL, respectively.

Cryo-EM grid preparation

Purified AdiC and GPR from SEC (3 µL) were applied to glow-discharged (22.5 s at 15 mA, 200 V and 0.25 mbar) Quantifoil R1/2 200-mesh copper grids. After 30 s wait time, grids were vitrified using a Vitrobot Mark IV (100% humidity, 4°C, blot force -6, blot time 4 s) by plunging them into liquid ethane (-175°C).

Cryo-EM data acquisition and single particle analysis

Cryo-EM images were acquired on a Tecnai F20 transmission electron microscope (FEI) with a field emission gun operated at 200 kV and equipped with a Falcon III direct electron detector (Thermo Fisher Scientific). All cryo-EM data were automatically collected using the EPU software (Thermo Fisher Scientific). Briefly, movies of frozen-hydrated AdiC were collected in counting mode at a nominal magnification of 60,000×, corresponding to 1.684 Å per pixel, over a defocus range of -1.5 to -3.0 µm. Movies of GPR were acquired at a magnification of 80,000×, corresponding to 1.306 Å per pixel,

over the same defocus range. Micrographs were exposed for 2.5 s (dose-fractioned into 30 sub-frames) with a dose rate of 1.19 $e^{-}/Å^2$ per frame, amounting to a total accumulated dose of 35.7 $e^{-}/Å^2$. In total, 205 and 323 movies were collected for AdiC and GPR, respectively, which were then imported in cryoSPARC (v3.2.0) for single-particle analysis (Punjani et al., 2017). CTF estimation and beam-induced motion correction were performed using the patch implementation, followed by manual curation of the micrographs. The remaining movies were then subjected to blob picking and particle coordinates were extracted under binning using boxes of 200/96 and 400/120 pixels (box size/Fourier cropping) for AdiC and GPR, respectively. Successive rounds of 2D classification and selection of high-quality class averages yielded well discernible particle populations corresponding to various oligomeric states. The latter were separately subjected to *ab initio* 3D reconstruction, followed by homogenous refinement without imposing any symmetry.

Acknowledgements

Financial support from the University of Bern and the NCCR Molecular Systems Engineering is kindly acknowledged. Cryo-EM experiments were performed on equipment supported by the Microscopy Imaging Center (MIC), University of Bern, Switzerland. Stephan Hirschi is supported by a Postdoc.Mobility grant (No. 203042) by the Swiss National Science Foundation.

Declaration of competing Interest

The authors declare that they have no known competing financial interests or personal relationships that could have appeared to influence the work reported in this paper.

References

Bergeron, M.J., Boggavarapu, R., Meury, M., Ucurum, Z., Caron, L., Isenring, P., Hediger, M.A., Fotiadis D., 2011. Frog oocytes to unveil the structure and supramolecular organization of human transport proteins. PLoS ONE 6, e21901. https://doi.org/10.1371/journal.pone.0021901

Boggavarapu, R., Jeckelmann, J.-M., Harder, D., Schneider, P., Ucurum, Z., Hediger, M., Fotiadis D., 2013. Expression, purification and low-resolution structure of human vitamin C transporter SVCT1 (SLC23A1). PLoS ONE 8, e76427. https://doi.org/10.1371/journal.pone.0076427

Bolanos-Garcia, V.M., Davies, O.R., 2006. Structural analysis and classification of native proteins from *E. coli* commonly co-purified by immobilised metal affinity chromatography. Biochim. Biophys. Acta 1760, 1304–1313. https://doi.org/10.1016/j.bbagen.2006.03.027

Bornhorst, J.A., Falke, J.J., 2000. Purification of proteins using polyhistidine affinity tags. Methods Enzymol. 326, 245–254. https://doi.org/10.1016/s0076-6879(00)26058-8

Casagrande, F., Ratera, M., Schenk, A.D., Chami, M., Valencia, E., Lopez, J.M., Torrents, D., Engel, A., Palacin, M., Fotiadis, D., 2008. Projection structure of a member of the amino acid/polyamine/organocation transporter superfamily. J. Biol.

Chem. 283, 33240–8. https://doi.org/10.1074/jbc.M806917200

Grisshammer, R., Tucker, J., 1997. Quantitative evaluation of neurotensin receptor purification by immobilized metal affinity chromatography. Protein Expr. Purif. 11, 53–60. https://doi.org/10.1006/prep.1997.0766

Hemdan, E.S., Zhao, Y.J., Sulkowski, E., Porath, J., 1989. Surface topography of histidine residues: a facile probe by immobilized metal ion affinity chromatography. Proc. Natl. Acad. Sci. U. S. A. 86, 1811–1815. https://doi.org/10.1073/pnas.86.6.1811

Hirschi, S., Fotiadis, D., 2020. Purification of membrane proteins by affinity chromatography with on-column protease cleavage. Methods Mol. Biol. 2127, 139–150. https://doi.org/10.1007/978-1-0716-0373-4_10

Hirschi, S., Kalbermatter, D., Ucurum, Z., Fotiadis, D., 2020. Cryo-electron microscopic and X-ray crystallographic analysis of the light-driven proton pump proteorhodopsin reveals a pentameric assembly. J. Struct. Biol. X 4, 100024. https://doi.org/10.1016/j.yjsbx.2020.100024

Hirschi, S., Kalbermatter, D., Ucurum, Z., Lemmin, T., Fotiadis, D., 2021. Cryo-EM structure and dynamics of the green-light absorbing proteorhodopsin. Nat. Commun. 12, 4107. https://doi.org/10.1038/s41467-021-24429-6

Hochuli, E., Bannwarth, W., Döbeli, H., Gentz, R., Stüber, D., 1988. Genetic approach to facilitate purification of recombinant proteins with a novel metal chelate adsorbent. Nat. Biotechnol. 6, 1321–1325. https://doi.org/10.1038/nbt1188-1321

Ilgü, H., Jeckelmann, J.-M., Kalbermatter, D., Ucurum, Z., Lemmin, T., Fotiadis, D., 2021. High-resolution structure of the amino acid transporter AdiC reveals insights

into the role of water molecules and networks in oligomerization and substrate binding. BMC Biol. 19, 179. https://doi.org/10.1186/s12915-021-01102-4

Ilgü, H., Jeckelmann, J.-M., Gachet, M.S., Boggavarapu, R., Ucurum, Z., Gertsch, J., Fotiadis, D., 2014. Variation of the detergent-binding capacity and phospholipid content of membrane proteins when purified in different detergents. Biophys. J. 106, 1660–1670. https://doi.org/10.1016/j.bpj.2014.02.024

Kaur, J., Reinhardt, D.P., 2012. Immobilized metal affinity chromatography co-purifies TGF-β1 with histidine-tagged recombinant extracellular proteins. PLoS ONE 7, e48629. https://doi.org/10.1371/journal.pone.0048629

Kenig, M., Peternel, Š., Gaberc-Porekar, V., Menart, V., 2006. Influence of the protein oligomericity on final yield after affinity tag removal in purification of recombinant proteins. J. Chromatogr. A 1101, 293–306. https://doi.org/10.1016/j.chroma.2005.09.089

Kunji, E.R.S., Harding, M., Butler, P.J.G., Akamine, P., 2008. Determination of the molecular mass and dimensions of membrane proteins by size exclusion chromatography. Methods 46, 62–72. https://doi.org/10.1016/j.ymeth.2008.10.020

Mohanty, A.K., Wiener, M.C., 2004. Membrane protein expression and production: effects of polyhistidine tag length and position. Protein Expr. Purif. 33, 311–325. https://doi.org/10.1016/j.pep.2003.10.010

Pettersen, E.F., Goddard, T.D., Huang, C.C., Meng, E.C., Couch, G.S., Croll, T.I., Morris, J.H., Ferrin, T.E., 2021. UCSF ChimeraX: Structure visualization for researchers, educators, and developers. Protein Sci. 30, 70–82. https://doi.org/10.1002/pro.3943

Punjani, A., Rubinstein, J.L., Fleet, D.J., Brubaker, M.A., 2017. cryoSPARC: algorithms for rapid unsupervised cryo-EM structure determination. Nat. Methods 14, 290–296. https://doi.org/10.1038/nmeth.4169

Rath, A., Glibowicka, M., Nadeau, V.G., Chen, G., Deber, C.M., 2009. Detergent binding explains anomalous SDS-PAGE migration of membrane proteins. Proc. Natl. Acad. Sci. U. S. A. 106, 1760–1765. https://doi.org/10.1073/pnas.0813167106

Reig, N., del Rio, C., Casagrande, F., Ratera, M., Gelpí, J.L., Torrents, D., Henderson, P.J.F., Xie, H., Baldwin, S.A., Zorzano, A., Fotiadis, D., Palacín, M., 2007. Functional and structural characterization of the first prokaryotic member of the L-amino acid transporter (LAT) family: a model for APC transporters. J. Biol. Chem. 282, 13270–13281. https://doi.org/10.1074/jbc.M610695200

Schmitt, J., Hess, H., Stunnenberg, H.G., 1993. Affinity purification of histidine-tagged proteins. Mol. Biol. Rep. 18, 223–230. https://doi.org/10.1007/BF01674434

Waugh, D.S., 2011. An overview of enzymatic reagents for the removal of affinity tags. Protein Expr. Purif. 80, 283–293. https://doi.org/10.1016/j.pep.2011.08.005

Weitz, D., Harder, D., Casagrande, F., Fotiadis, D., Obrdlik, P., Kelety, B., Daniel, H., 2007. Functional and structural characterization of a prokaryotic peptide transporter with features similar to mammalian PEPT1. J. Biol. Chem. 282, 2832–2839. https://doi.org/10.1074/jbc.M604866200

Wülfing, C., Lombardero, J., Plückthun, A., 1994. An *Escherichia coli* protein consisting of a domain homologous to FK506-binding proteins (FKBP) and a new metal binding motif. J. Biol. Chem. 269, 2895–901.

Figure legends

Figure 1: SEC analysis of AdiC variants. SEC profiles (Superose 6 10/300) and 13.5% SDS-polyacrylamide gels of IMAC-purified His_{10}-tagged AdiC eluted with L-histidine (a) or after proteolytic removal of the His_{10}-tag (b). His_{10}-tagged AdiC analysed in SEC buffer containing 200 mM L-histidine (c) or after complete removal of L-histidine by desalting analysed in SEC buffer without L-histidine (d). The void (V_0) and elution volumes of MW standard proteins are indicated: thyroglobulin (TG, 669 kDa), ferritin (FT, 440 kDa), aldolase (AD, 158 kDa) and conalbumin (CA, 75 kDa).

Figure 2: SEC analysis of GPR variants. SEC profiles (Superose 6 10/300) and 13.5% SDS-polyacrylamide gels of IMAC-purified His_{10}-tagged (a) and His_5-tagged GPR (b) eluted with L-histidine. (c) His_{10}-tagged GPR analysed in SEC buffer containing 200 mM L-histidine. The void (V_0) and elution volumes of MW standard proteins are indicated: thyroglobulin (TG, 669 kDa), ferritin (FT, 440 kDa), aldolase (AD, 158 kDa) and conalbumin (CA, 75 kDa).

Figure 3: Single particle cryo-EM analysis of AdiC oligomers. (a) Representative electron micrograph of DM-solubilized, purified AdiC. Discernible dimers and tetramers are indicated with magenta and blue circles, respectively. Insets display three-fold magnified examples of the corresponding particles. (b) Typical 2D class averages of dimeric and tetrameric AdiC. Corresponding 3D reconstructions with fitted AdiC models (PDB ID: 7O82) (Ilgü et al., 2021) for the dimeric (c) and tetrameric map (d). AdiC monomers are coloured in blue and yellow. An asterisk indicates where the C-terminal His-tags interact to form an interface between the AdiC dimers. Figure was prepared using UCSF ChimeraX (Pettersen et al., 2021).

Figure 4: Single particle cryo-EM analysis of GPR oligomers. (a) Representative electron micrograph of Cymal-5-solubilized, purified GPR. Discernible pentamers, decamers and pentadecamers are indicated with red, blue and green circles, respectively. Insets display three-fold magnified examples of the corresponding particles. (b) Typical 2D class averages of pentameric, decameric and pentadecameric GPR particles. Corresponding 3D reconstructions with fitted GPR models (PDB ID: 7B03) (Hirschi et al., 2021) for the pentameric (c), decameric (d) and pentadecameric maps (e). GPR monomers are coloured individually. An asterisk indicates where the C-terminal His-tags interact to form an interface between the GPR pentamers. Figure was prepared using UCSF ChimeraX (Pettersen et al., 2021).

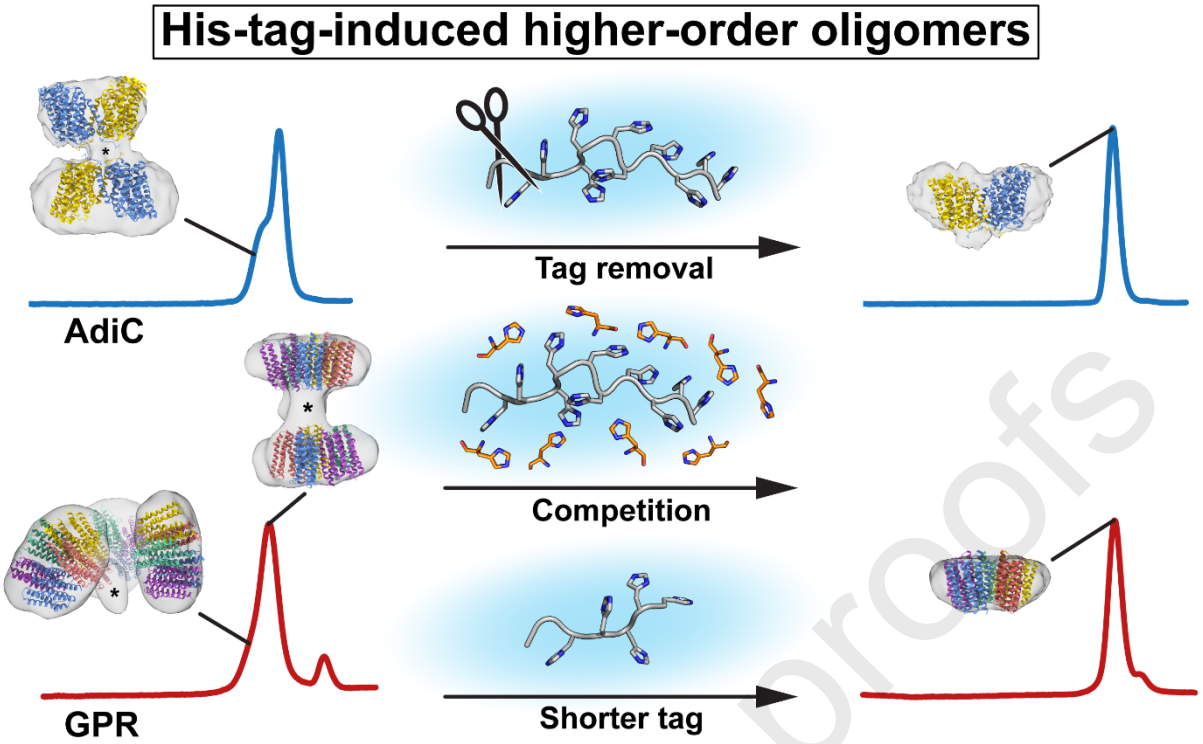

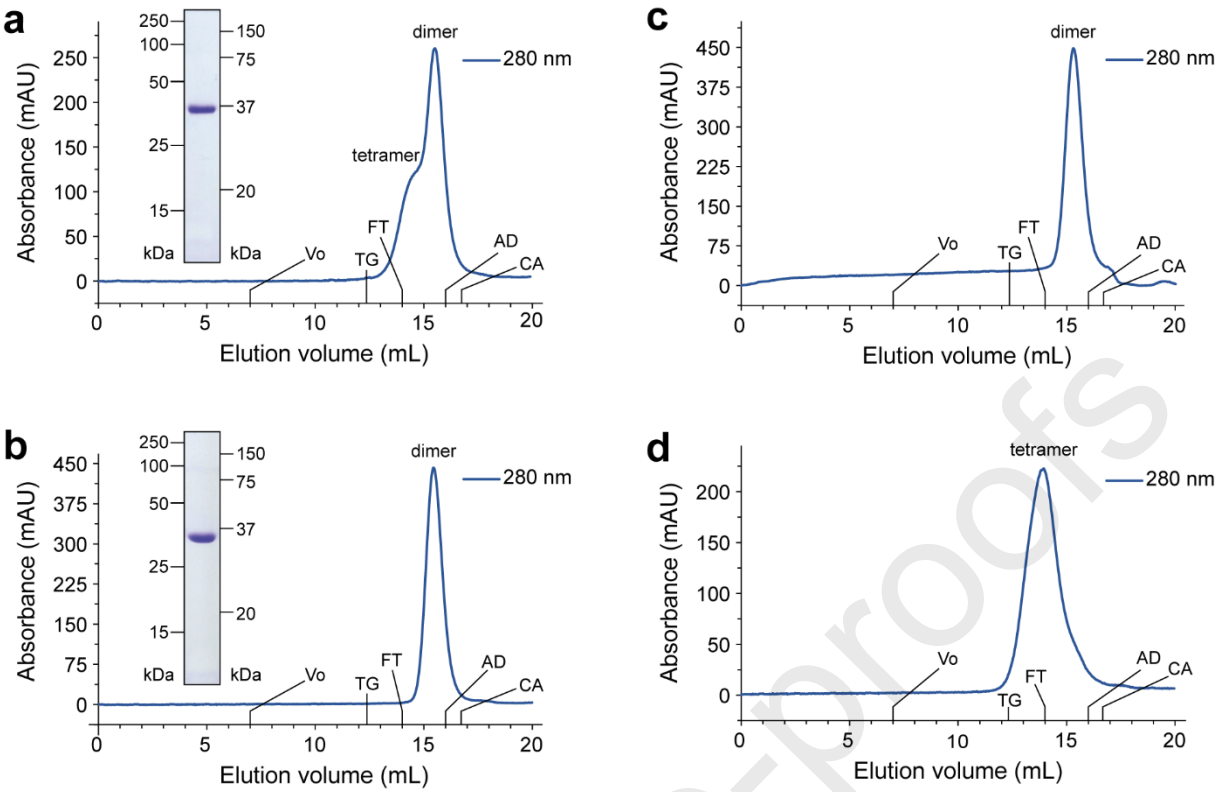

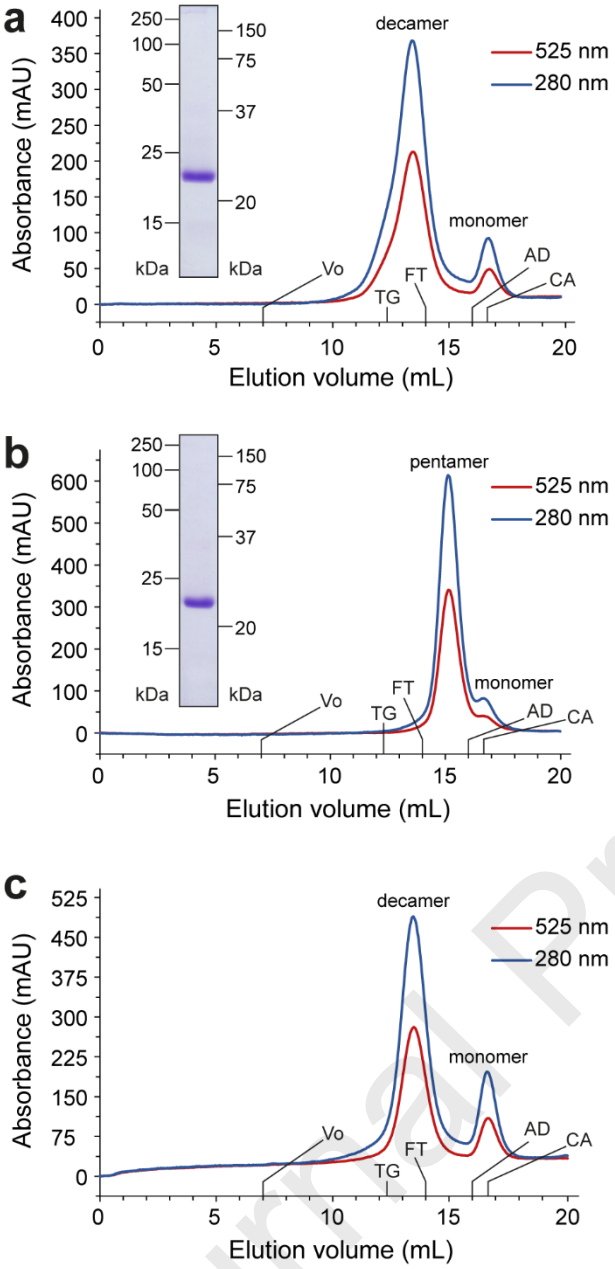

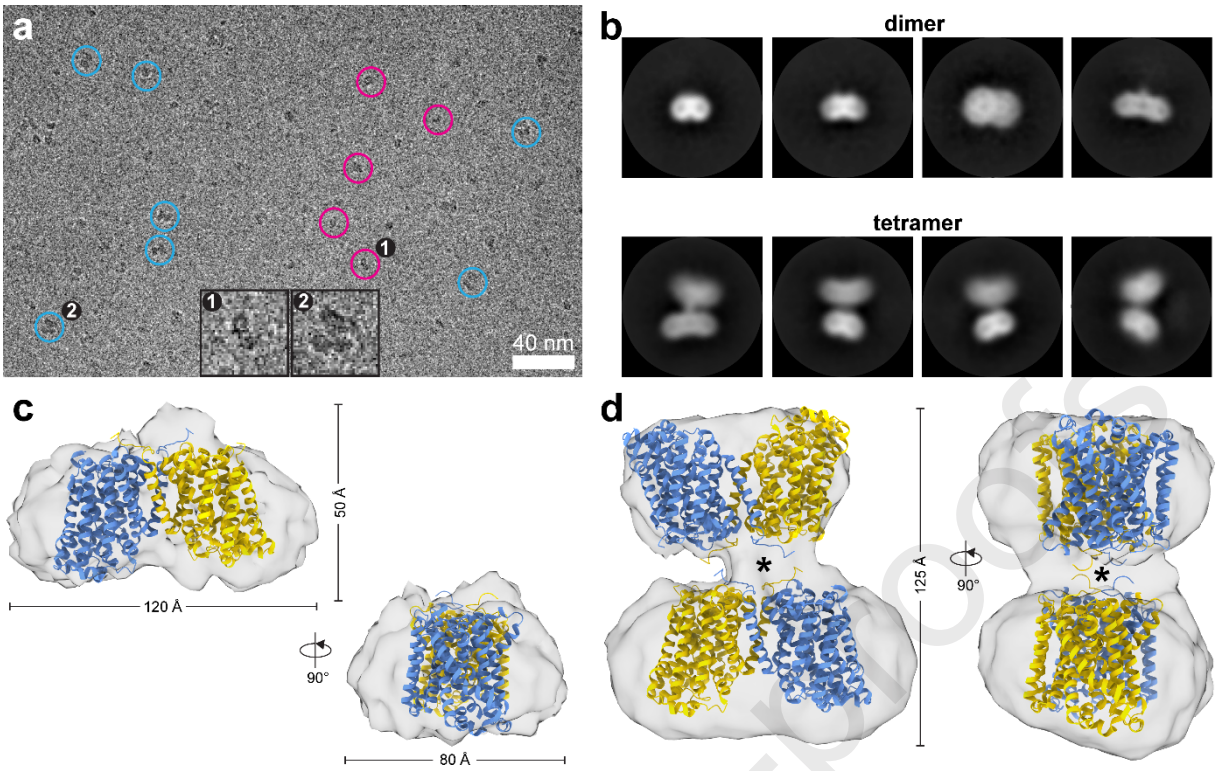

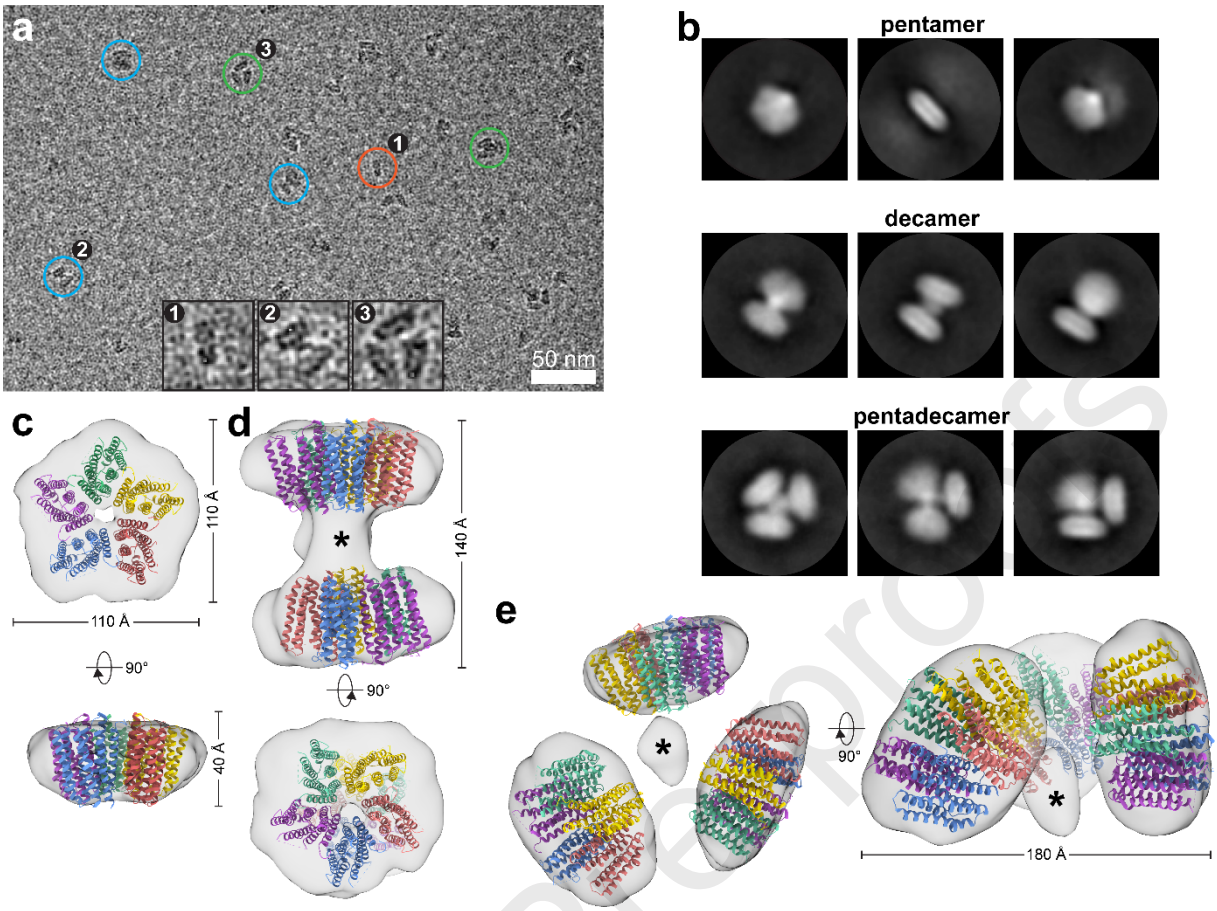

Declaration of interests

☒ The authors declare that they have no known competing financial interests or personal relationships that could have appeared to influence the work reported in this paper.

☐ The authors declare the following financial interests/personal relationships which may be considered as potential competing interests:

Author contributions

S.H. and D.F. conceived and designed the experiments. N.A., P.R., Z.U. and S.H. performed the experiments. N.A., P.R., D.F. and S.H. analyzed the data and wrote the manuscript. All authors contributed to manuscript revision and approved the final version.

Highlights

- Analysis of His_{10}-tagged membrane proteins AdiC and GPR by size exclusion chromatography (SEC) reveals formation of non-physiological higher-order oligomers
- SEC experiments demonstrate that higher-order oligomer formation is mediated by His-tags and mainly depends on tag length
- Single particle cryo-EM analysis offers structural insights into the three-dimensional arrangement of higher-order oligomers and their interactions via His-tags
- Higher-order oligomers are identified as tetrameric AdiC as well as decameric and pentadecameric GPR assemblies